Polymer Chemistry

A Tunable One-Pot Three-Component Synthesis of an 125I and Gd-Labelled Star Polymer Nanoparticle for Hybrid Imaging with MRI and Nuclear Medicine

SCHOLARONE™
Manuscripts

Polymer Chemistry

ARTICLE

A Tunable One-Pot Three-Component Synthesis of an ^{125}I and Gd-Labelled Star Polymer Nanoparticle for Hybrid Imaging with MRI and Nuclear Medicine

Lars Esser,[a] Nigel A. Lengkeek,[b] Bradford A. Moffat,[c] Mai N. Vu,[a] Ivan Greguric,[b] John F. Quinn,[a] Thomas P. Davis*[a,d] and Michael R. Whittaker*[a]

The successful treatment of a disease via individualized treatment protocols relies on an early and accurate diagnosis. Advances to imaging hardware, such as hybrid PET/MRI scanners, have overcome the inherit disadvantages associated with the individual imaging modality. However, well-designed multimodal contrast agents are essential to optimally exploit hybrid PET/MRI systems. Herein, we show that core-cross-linked azide-functional star polymer nanoparticles can be simultaneously labelled with a radioisotope (radioiodine) and a clinically-used MRI contrast agent (Gd-DOTA) by exploiting an elegant copper-catalyzed one-pot three-component reaction creating an iodotriazole. The nanoparticles have a longitudinal relaxivity of 5.7 $mM^{-1}s^{-1}$ at 7 T (as compared to 3.8 $mM^{-1}s^{-1}$ for commercially available Gd-DTPA), and a radiochemical yield of 58% was achieved. Furthermore, we show that the radioiodine content can be fine-tuned without affecting the final Gd-DOTA loading. While we have demonstrated the versatility of the approach with ^{125}I, an isotope widely used in biological research, the availability of various radioiodine isotopes enables potential applications in SPECT (^{123}I), PET ([124]I) and in theranostics by combining radioimmunotherapy (^{131}I) with MRI.

Introduction

An early accurate diagnosis of disease is essential to improve the chance of a successful treatment outcome via individualized treatment protocols. The current single-modality imaging methods tend to be inadequate due to the limitations of each technology[1], resulting in the development of multimodality imaging instruments such as SPECT/CT[2], PET/CT[3] and more recently PET/MRI[4,5] to overcome the disadvantages of each, thus maximizing their combined potential.[6] For example, PET offers a very high sensitivity (pico-molar range) and is quantifiable[7] but has a relatively low spatial resolution, whereas MRI provides a high resolution (down to 50 μm), excellent soft tissue contrast and physiological information, but has a relatively low sensitivity.[1,8] The hybrid PET/MRI system offers the additional benefit of a great reduction of radiation dose as compared to the current clinically used PET/CT.[9] As a consequence, after being commercially introduced in 2011, 70 PET/MRI systems were already operational worldwide by June 2015.[10]

However, in addition to the technological advances of the imaging hardware, the development of nanoparticle-based imaging probes is crucial for effective multimodal diagnostics and to fully exploit the benefits of PET/MRI.[11] To this end PET/MRI dual-mode probes have emerged in the literature.[12-18] To date PET/MRI nanoparticles have been primarily based on the combination of PET isotopes with superparamagnetic iron oxide (SPIO) nanoparticles, however this results in a hypointense MRI contrast that can be difficult to interpret. Moreover, SPIOs have failed to become established in the clinical setting.[19] In contrast, only a few studies have reported the use of clinically-used gadolinium MRI contrast agents in PET/MRI probes and these were predominantly focused on small-molecule probes.[20-22] Additionally, several studies also investigated bimodal SPECT/MRI nanoparticles, where the radioisotope was utilized to increase the imaging sensitivity or employed to address the essential question of the fate of the nanoparticles and their degradation products.[23-25]

Here we report a novel approach towards the synthesis of a bimodal PET/MRI imaging agent based on a core-cross-linked star polymer nanoparticle.[26-28] A copper-catalysed one-pot three component reaction[29,30] was optimized to simultaneously introduce both a gadolinium-chelate (for MRI) and radioiodine onto the azide-functionalized nanoparticle. The gadolinium-chelate was selected due to its familiarity and proven track record in clinical practice,[31] whereas the existence of numerous isotopes of radioiodine enable multiple applications: SPECT (^{123}I), PET ([124]I), biological research (^{125}I),

a. ARC Centre of Excellence in Convergent Bio-Nano Science & Technology, Monash Institute of Pharmaceutical Sciences, Monash University, Parkville, VIC 3052, Australia.
b. Australian Nuclear Science and Technology Organisation (ANSTO), Kirrawee DC, NSW 2232, Australia.
c. Melbourne Brain Centre, The University of Melbourne, Parkville, VIC 3050, Australia.
d. Department of Chemistry, University of Warwick, Coventry CV4 7AL, United Kingdom.
† Electronic Supplementary Information (ESI) available: See DOI: 10.1039/x0xx00000x

and radiotherapy (^{131}I).[30] Additionally the relatively long half-life of ^{124}I (4.2 days) is beneficial in long circulating nanoparticles as compared to other PET radioisotopes such as ^{18}F (110 min) and ^{64}Cu (12.7 h).

Experimental methods

Full experimental details are presented in the ESI.†

Results

We started with the synthesis of the azide-functional core-cross-linked star polymer nanoparticles (see Scheme 1). These dendrimer-like nanoparticles consist of numerous linear polymers (arms) fused at a central core and can be synthesized using reversible-deactivation radical polymerization methods with a high level of control over architecture and functionality.[26] Compared to dendrimers, star polymers can be synthesized with fewer facile reaction steps, which significantly simplifies the synthesis process while maintaining their desirable in vivo characteristics.[32] The azide groups were introduced after the synthesis of the star polymer to avoid the use of a potentially dangerous azido-containing comonomer.

Synthesis of P(VBC-co-OEGA) arm polymer.

First, a linear copolymer consisting of 4-vinylbenzyl chloride (4-VBC) and oligo(ethylene glycol) methyl ether acrylate (OEGA, average M_n 480 g mol^{-1}) was synthesized via RAFT polymerization. The use of arm-confined functionality was chosen as we had previously shown this would ensure the highest possible molecular MRI relaxivity.[27,33] The polymerization was carried out at 70 °C and the polymer molecular weight and composition were optimized to contain a molecular weight of around 10,000 g mol^{-1} and five functional chloride groups by varying solvents, molar feed ratios, concentration and reaction time (see Table S1 and

Scheme 1. Synthesis pathway for Gd-DOTA/radioiodine labelled star polymer nanoparticle.

Figure 1A). The polymer was purified by precipitation in diethyl ether : petroleum spirit (1 : 1 v/v).
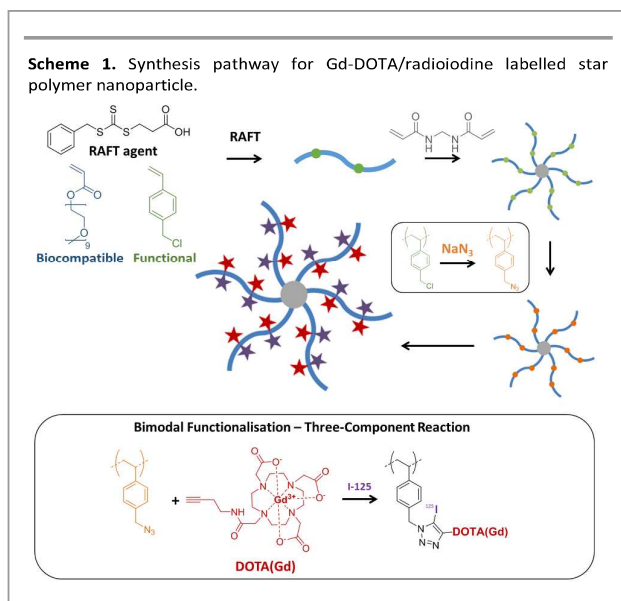
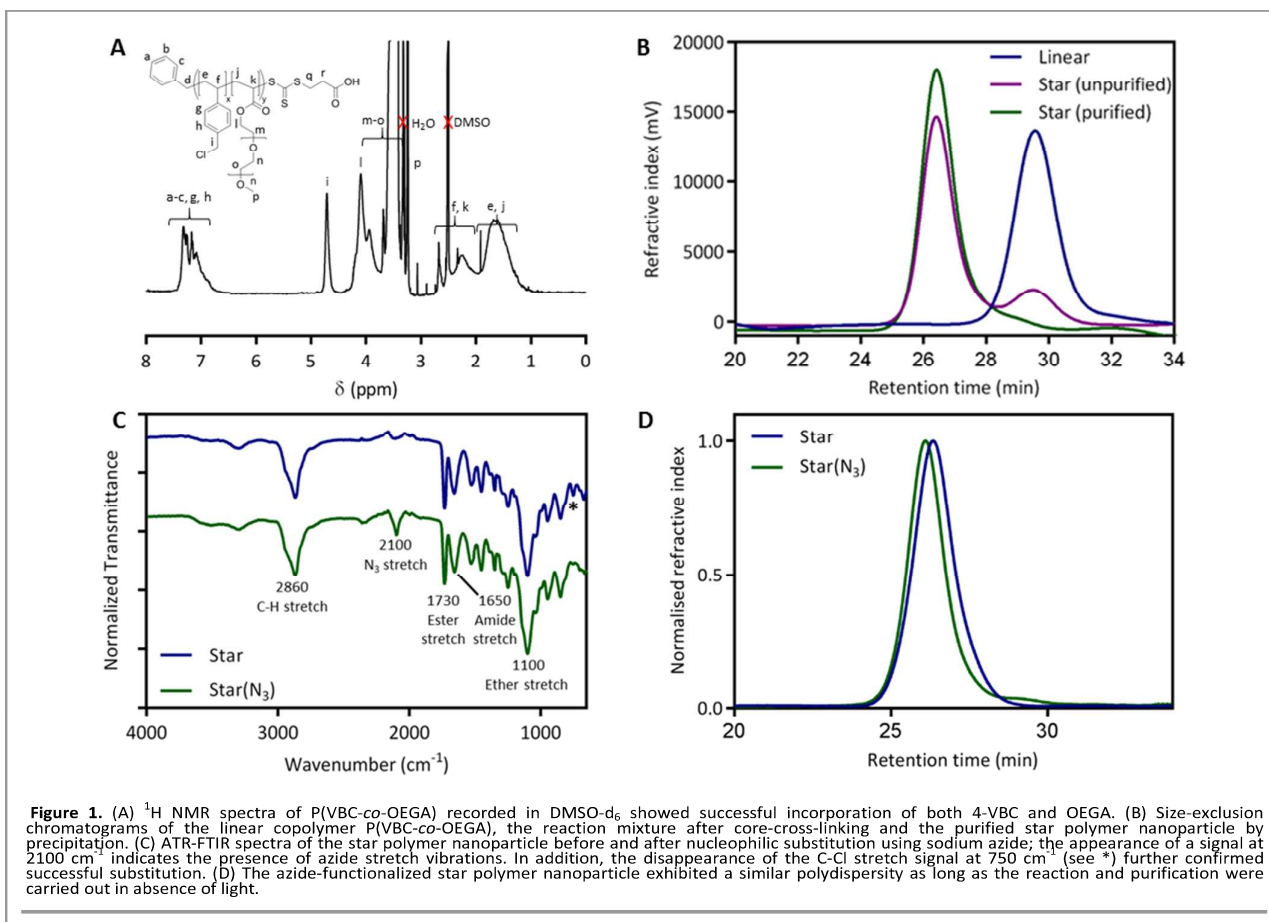### Synthesis of core-cross-linked star polymer nanoparticle

Core-cross-linked star polymer nanoparticles were obtained by chain-extending the copolymer P(VBC-co-OEGA) arm with a cross-linker, i.e. N,N'-methylenebis(acrylamide). The molecular weight (and therefore the hydrodynamic size) can be easily tuned by changing the cross-linker concentration.[34] Star polymer nanoparticles were successfully obtained with a low polydispersity and a number-average molecular weight between 55,000 and 155,000 g mol^{-1} (see Table S2, Figure S1-2). We did observe incomplete arm-to-star conversions in SEC, but rigorous purification by a carefully designed precipitation method (diethyl ether/chloroform (12:1 v/v)) resulted in the isolation of pure star products at high yields (see Figure 1b). The incomplete conversion is most likely caused by disproportionation and bimolecular termination of the propagating macro(radicals), leading to the formation of "dead" chains.[26]

Preparation of azide-functional star polymer nanoparticle

The azide functionality was introduced to the polymer nanoparticle via nucleophilic substitution of the chloride by azide, followed by purification by dialysis. The successful introduction of the azide moiety was confirmed by ATR-FTIR and ^{1}H NMR. ATR-FTIR showed the appearance of a signal at 2100 cm^{-1} (azide stretch vibrations, see Figure 1C) and the disappearance of the C-Cl stretch signal at 750 cm^{-1} indicated full conversion, while ^{1}H NMR showed an upfield shift of the benzylic proton signal from δ 4.55 to 4.30 ppm, also indicative of full conversion to azide (see Figure S3). In preliminary experiments star-star nanoparticle coupling was observed after lyophilization, as indicated by a high molecular weight shoulder in SEC (Đ > 2) (see Figure S4). The star-star coupling was attributed to azide photo-cross-linking by UV irradiation, which was further augmented by concentrating the solution.[36] This could be prevented by carrying out all purifications in darkness, and storing the products in acetone until required. SEC showed no significant increase in molecular weight nor polydispersity (see Figure 1D, Table S3), and the star polymer nanoparticles were stable for at least 6 months (see Figure S5).

In this article the star polymer nanoparticle with a number-average hydrodynamic radius of 10 nm and a M_n of 56,000 g mol^{-1} was employed as the platform for further investigation. This star polymer was selected as PEGylated star polymers with a relatively similar size and molecular weight (64,000 g mol^{-1}) were previously shown to have a long blood circulation time and a similar pharmaceutical behavior to PEGylated dendrimers.[21] The employed star polymer contained 5 - 6 arms with, on average, 29 functional groups per macromolecule.

Figure 1. (A) ^{1}H NMR spectra of P(VBC-*co*-OEGA) recorded in DMSO-d$_6$ showed successful incorporation of both 4-VBC and OEGA. (B) Size-exclusion chromatograms of the linear copolymer P(VBC-*co*-OEGA), the reaction mixture after core-cross-linking and the purified star polymer nanoparticle by precipitation. (C) ATR-FTIR spectra of the star polymer nanoparticle before and after nucleophilic substitution using sodium azide; the appearance of a signal at 2100 cm^{-1} indicates the presence of azide stretch vibrations. In addition, the disappearance of the C-Cl stretch signal at 750 cm^{-1} (see *) further confirmed successful substitution. (D) The azide-functionalized star polymer nanoparticle exhibited a similar polydispersity as long as the reaction and purification were carried out in absence of light.

Optimization of the three-component "click" reaction for iodine labelling

The three-component "click" reaction was based on earlier studies by the Årstad group in which a one-pot, three-component, copper(II)-mediated reaction of azide, alkyne, and [^{125}I]iodine yielded 5-[^{125}I]iodo-1,2,3-triazoles (see Scheme S1), although this study was limited to reactions containing small molecules.[29, 30] In their first study the reactivity of azides and alkynes bearing aliphatic, benzylic, aromatic, and heterocyclic moieties was investigated[29] and in a follow-up study the three-component reaction was employed to combine a fluorescent group, a radioactive element, and a group for bioconjugation to a targeting antibody.[30]

In the current study, the three-component reaction was applied to the highly complex star polymer nanoparticle. Initially, a simplified system was employed to optimize the translation of the three-component reaction to the star polymer nanoparticle platform. A linear azide-functional copolymer P(VBAz-*co*-OEGA) (see Table S2) was utilized in combination with a simple 3-butyn-1-ol alkyne and sodium iodide was used as a source for cold iodine. DMSO : water (10 : 1) was selected as reaction medium, and the amount of water (radioiodine is supplied in water) was kept to a minimum as an increasing water content had been found to have a detrimental effect on the overall radiochemical yield (RCY).[29]

The reaction time was set to 16 hours to take into account potential steric hindrance that could negatively affect the reaction rate. During these initial optimization experiments, cold sodium iodide was used and reactions were carried out on a 10 μmol (azide) scale. After reaction, the purified product was obtained by dialysis (against DMF and water) and analyzed by ^{1}H NMR, ATR-FTIR, and SEC.

^{1}H NMR spectra showed the presence of NMR signals that could be attributed to the successful triazole formation (see Figure S6), however the existence of a chemical shift at 7.86 ppm indicated that a proton was incorporated in the triazole. However closer investigation of the intensities of the different signals confirmed the partial formation of iodinated triazole with a yield of approximately 39%. This was further validated by the observed splitting of the other NMR signals, signifying the presence of a mixed chemical environment containing both triazoles and iodotriazoles. Finally, the disappearance of the azidomethyl signal at 4.40 ppm indicated full "click" conversion of this group, which was corroborated by the disappearance of the azide stretch signal at 2100 cm^{-1} in ATR-FTIR (see Figure S7A). Size-exclusion chromatography revealed a small change in retention time indicating the expected higher molecular weights, and the low polydispersity was maintained (M_n/M_w = 1.16, see Figure S7B).

As literature reported that the formation of the non-iodinated triazole was sluggish and the azide and alkyne would remain largely intact in the reaction mixture[29], the same reaction was repeated in absence of sodium iodine. Surprisingly full triazole formation was achieved, indicating that the macromolecular system combined with modified reaction conditions resulted in modified reaction kinetics. We further investigated this by adding different equivalents of sodium iodide, and indeed when increasing from 0.5 to 1.5 equivalents, the iodotriazole became more dominant: increasing from 20% to 49%. This provides the opportunity to fine-tune the iodine content of the macromolecule without limiting the number of conjugated alkyne groups (i.e. gadolinium chelates for MRI) in the macromolecular architecture, considering that much less radioiodine is required in the final multimodal nanoparticle c.f. Gd due to the much higher sensitivity of PET. At the same time, full formation of iodotriazole could not be achieved as no further increase in iodotriazole formation was observed even when 5 equivalents of sodium iodide was added (see Table S4).

Next, the one-pot three-component reaction was studied for the more complex star polymer nanoparticle. The same reaction conditions were applied and reactions were again carried out on 10 μmol (azide) scale using 3-butyn-1-ol as a test alkyne. ^{1}H NMR demonstrated successful triazole formation (see Figure 2) and analysis of the signal intensities again confirmed the formation of both iodotriazole and non-iodinated triazole. ATR-FTIR validated full conversion of the azide groups (see Figure S8A), while a small change in retention time was observed in SEC with low polydispersity maintained (M_w/M_n = 1.20, see Figure S8B) . Similar to the linear polymer, the triazole was also formed in the absence of sodium iodide, and the ratio of iodotriazole versus non-iodinated triazole could be varied by changing the amount of added sodium iodide to a maximum of around 46% using the optimized reaction conditions (see Table S5).

In summary, the star polymer and linear polymer nanoparticles were both successfully labelled with cold iodine using 3-butyn-1-ol as alkyne. The three-component reaction was carried out in DMSO for 16 hours at 60 °C to improve solubility and reaction efficacy. Importantly, both iodotriazole and non-iodinated triazole were formed simultaneously and
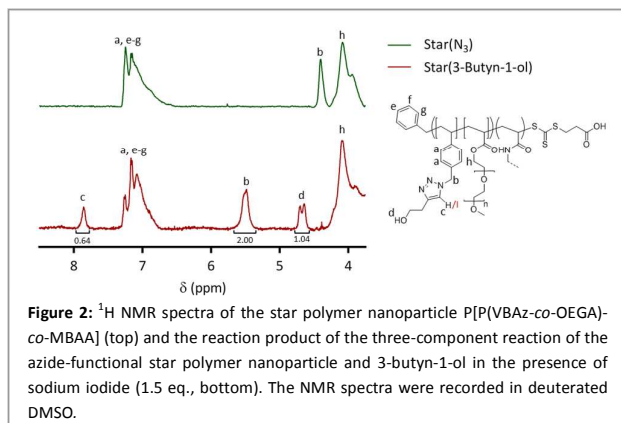
Figure 2: ^{1}H NMR spectra of the star polymer nanoparticle P[P(VBAz-co-OEGA)-co-MBAA] (top) and the reaction product of the three-component reaction of the azide-functional star polymer nanoparticle and 3-butyn-1-ol in the presence of sodium iodide (1.5 eq., bottom). The NMR spectra were recorded in deuterated DMSO.

Scheme 2. Synthesis of butyne-functional gadolinium-chelate in two reaction steps.
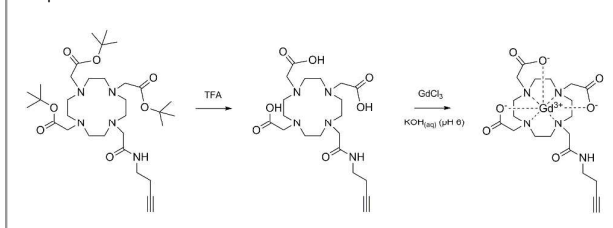
the ratio could be fine-tuned by changing the amount of sodium iodide to a maximum of around 50%.

Optimization of Gd-DOTA / cold-iodine labelled star polymer nanoparticles

After successfully optimizing the three-component reaction for the linear and star polymer and a small alkyne (3-butyn-1-ol), we studied the reaction with the more complex butyne-functional gadolinium chelate (butyne-Gd-DOTA) to open the pathway to bimodal MRI/PET polymer star nanoparticles. Butyne-Gd-DOTA was synthesized in two steps (see Scheme 2). First, the commercially available butyne-DOTA-tris(t-butyl ester) was deprotected overnight with trifluoroacetic acid (TFA), followed by removal of residual TFA and the volatile side products by evaporation under vacuum. The deprotection was confirmed by disappearance of the tert-butyl ^{1}H NMR proton signal (at δ 1.51 ppm, see Figure S9) and the presence of one main product in ultra-high performance liquid chromatography - mass spectroscopy (UHPLC-MS) with an m/z of 456.2[M+H][+] (see Figure S10A). In the second step, the chelate was incubated in the presence of gadolinium chloride under slightly acidic conditions (pH 6) at 50 °C for 24 hours to facilitate complexation. Free gadolinium was removed using Chelex 100, followed by filtration and lyophilization to obtain an off-white solid. The final compound, butyne-Gd-DOTA, was successfully obtained and characterized by UHPLC-MS with an m/z of 610.2 [M + H][+] (see Figure S10B).

Next, the three-component reaction using butyne-Gd-DOTA was investigated with the previously employed conditions. However, the incorporation of Gd-DOTA into the star polymer nanoparticle was initially unsuccessful. Only trace levels of Gd were detected by inductively coupled plasma optical emission spectrometry (ICP-OES) and ensuing ATR-FTIR measurements showed no significant reduction of the azide peak at 2100 cm^{-1}.We assumed that the lower solubility of butyne-Gd-DOTA in DMSO at 60 °C strongly limited the reaction efficacy. As a consequence, different polar solvents were investigated, e.g. acetone, acetonitrile, N,N-dimethylacetamide, N,N-dimethylformamide, 1,4-dioxane, methanol, tetrahydrofuran and water, however none was found to be suitable for all reagents (azide-functional polymers, butyne-Gd-DOTA, Cu(II)Cl2, triethylamine, and sodium iodide). Therefore, we attempted to improve the solubility of butyne-Gd-DOTA by increasing the temperature and determined that butyne-Gd-DOTA was more soluble in DMSO at 90 °C. However when the three-component reaction

was repeated under these conditions limited reaction was still observed. Serendipitously, however, we discovered that we could drive the three-component reaction to completion by concentrating the reaction mixture during the reaction; this was achieved by a combination of evaporation and condensation near the top of the reaction vessel. As the reaction volume was very small (80 µl), the removal of solvent from the reaction by in situ evaporation-condensation had a large effect on the solvent volume and thus reagent concentration (see Scheme S2). We successfully used these conditions for the star polymer nanoparticle with the final conjugation efficacy determined to be 85% by ICP-AES (25 Gd/star). No star-star nanoparticle coupling was observed in the SEC (See Figure S11) and dynamic light scattering (DLS) indicated a number-average hydrodynamic diameter of 10 nm (See Figure S12), which was confirmed by transmission electron microscopy (average size 9 nm, See Figure S13).

Analysis of MRI relaxivity properties of bimodal star nanoparticles

Cold iodine was used for this experiment as the presence of radioactivity could potentially result in safety issues during the determination of the gadolinium content by ICP-AES. To increase the amount of usable material, the reaction was also successfully scaled up by increasing the concentration four-fold while maintaining conjugation efficiency. Increasing concentration was preferred over increasing volume as the latter affected the evaporation/condensation process, leading to a limited increase in concentration over time.

The MRI properties of the gadolinium-labelled polymer nanoparticles were investigated using a 7-Tesla whole-body MRI scanner (MAGNETON 7T, Siemens). First, dilution series in water of (i) Gd-DOTA/iodine labelled star polymer nanoparticles, (ii) butyne-Gd-DOTA and (iii) Gd-DOTA (the latter two as controls) were prepared in a 96-well plate for high-throughput measurement. The space between the wells was then filled with 3% agarose to minimize susceptibility effects caused by water-air interfaces. For the determination of the T_1 relaxation rates (R_1), an inversion recovery sequence was used with different inversion times, ranging from 22 to 4000 ms (repetition time / echo time = 5000 / 11.5 ms). The

Table 1. T_1 relaxivity (r_1) at 7 T for the star polymer nanoparticle as compared to butyne-Gd-DOTA and commercial-available Magnevist (Gd-DTPA).

| Compound	r_1 ($mM^{-1}s^{-1}$) ionic	Gd per molecule	r_1 ($mM^{-1}s^{-1}$) molecular
Gd-DOTA-I-Star	5.7	25	142.5
Butyne-Gd-DOTA	3.4	1	3.4
Gd-DTPA (Magnevist)	3.8	1	3.8

respective relaxation rates were then plotted as a function of the gadolinium concentration and a linear least-squares analysis (GraphPad Prism) was used to determine the r_1 relaxivity (See Figure 3A, S14 and Table 1). This gives an indication of the efficiency of contrast enhancement by MRI contrast agents. The higher the relaxivity, the more efficient the contrast agent is in shortening the relaxation times and thus enhancing contrast.

The r_1 relaxivity of the Gd-DOTA/iodine labelled star polymer nanoparticle was 5.7 $mM^{-1}s^{-1}$ at 7 T which is 72% higher than the chelate (3.4 $mM^{-1}s^{-1}$) and 50% higher than commercially available Gd-DTPA (Magnevist, 3.8 $mM^{-1}s^{-1}$, see Figure 3A and Table 1). The higher relaxivity can be attributed to the slower rotational dynamics of the larger macromolecule, which results in a more optimal relaxation and thus higher r_1 relaxivity.[33] These results confirmed one of the main advantages of using a large macromolecule as compared to a small molecule for MRI contrast-enhanced imaging. No previous measurements were performed on star polymer nanoparticles at 7 T, however measurements of Gd-DOTA labelled star polymers at 9.4 T showed values in the range of 4.7 – 5.2 $mM^{-1}s^{-1}$.[27] Furthermore, Gd-DOTA labelled polymeric micelles exhibited an r_1 of 5.3 $mM^{-1}s^{-1}$ at 7 T,[37] while Holbrook *et al.* reported a maximal r_1 of 4.7 $mM^{-1}s^{-1}$ for Gd-DTPA labelled gold nanoparticles at 7 T.[38] Finally, the value for the Gd chelate alone was similar to reported in literature.[39]

Cell viability

The cell viability of the star polymer nanoparticles was tested in human umbilical vein endothelial cells (HUVECs, Lonza)

Figure 3. (A) Longitudinal relaxation rates (R_1) plotted against gadolinium concentration for the Gd-DOTA/I labelled star polymer nanoparticle ($R^2 \geq 0.9986$). Butyne-Gd-DOTA and Gd-DOTA (Magnevist) were examined as controls. (B) Cell viability study for the HUVEC cell line.
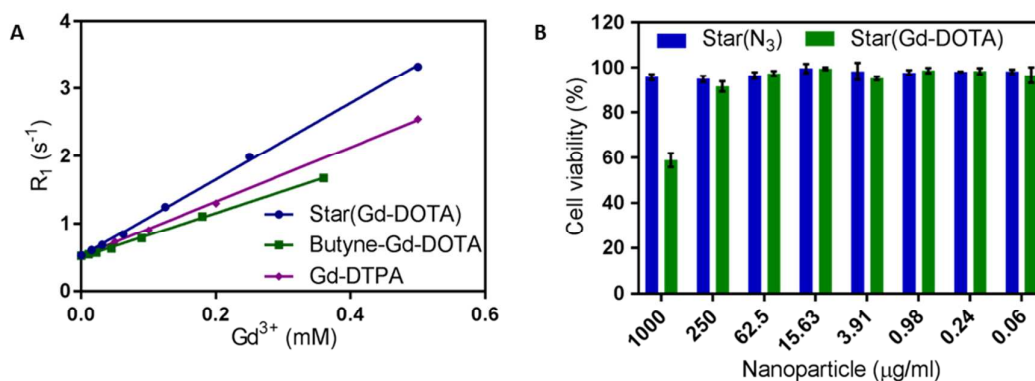
using alamarBlue reagent. No cytotoxicity was observed below 250 µg/ml (see Figure 3B): a concentration far higher than any expected to be used clinically.
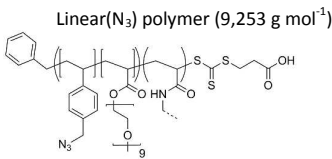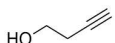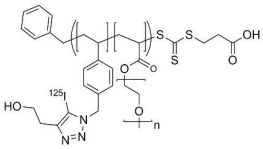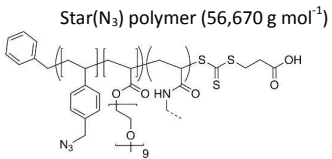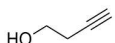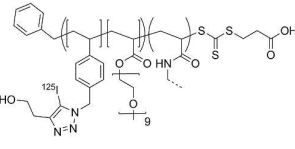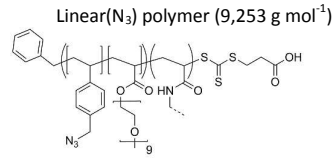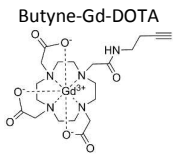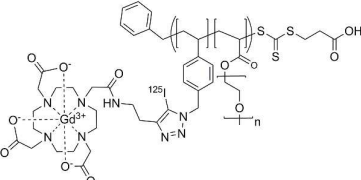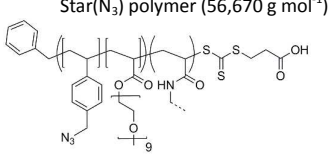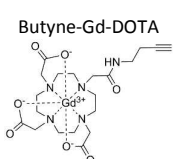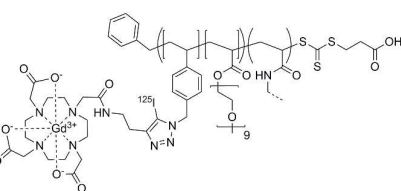
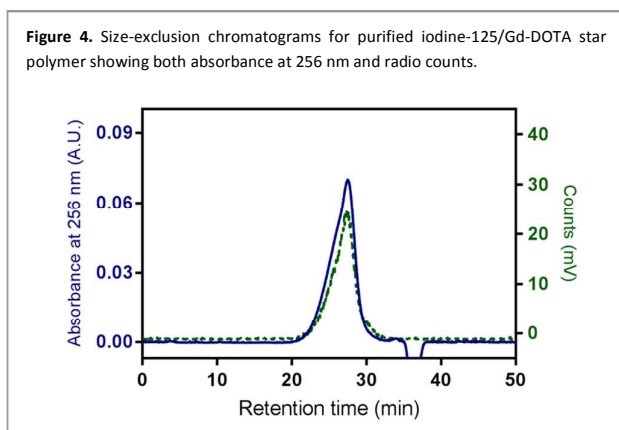### Radiolabelling of polymer nanoparticles

Iodine-125 was selected to investigate radioiodine labelling as it has a long half-life (59.4 days) and is relatively safe to handle due to the very low gamma energy (35 keV) of the emitted radiation.[40] The labelling was assessed using an aqueous size-exclusion chromatography system comprising a refractive index detector, an absorbance detector and a radio-HPLC detector. An aqueous buffer (0.10 mM phosphate buffer, 0.1 M sodium nitrate (pH 7)) containing 20% DMSO was employed as the mobile phase. DMSO was incorporated to limit hydrophobic interactions with the ultrahydrogel column. Sodium iodine-125 was clearly detectable on the radio-HPLC detector and did not appear to have any irreversible interactions with the column (see Figure S15). Furthermore, the radiochemical substance could also be identified using the refractive index detector. However as expected, no

absorbance was detected at 256 nm, providing a second method to differentiate polymer from free iodine-125. As iodine-125 had a different retention time than the polymer, radio-HPLC could be used to assess the radiochemical yield.

We first investigated the radioiodine labelling using 3-butyn-1-ol with either linear polymer P(VBAz-*co*-OEGA) or star polymer nanoparticle and [^{125}I]sodium iodide. Reactions were carried out for 16 hours at 60 °C on a 2.3 µmol (azide group) scale in DMSO (160 µL) using 2.0 MBq iodine-125. The reactions were directly analyzed by aqueous size-exclusion chromatography, followed by purification by centrifugal filtration (MWCO 3,500) and re-analysis by aqueous SEC. Aqueous SEC showed a shift to shorter retention times for both the linear and star polymer nanoparticle after reaction. This was previously observed for the three-component reactions with cold iodine, and likely indicates a higher molecular weight and thus successful conjugation (see Figure S16). The refractive index detector showed the presence of two main peaks designated as the nanoparticles and free iodine, respectively (see Figure S17, top) and the nanoparticles were clearly noticeable when measuring the absorbance at

Table 2. Radiochemical yields (RCY) for the three-component reaction between linear polymers or star polymer nanoparticles with 3-butyn-1-ol or butyne-Gd-DOTA and iodine-125. The reactions were performed in DMSO for 16 hours at 60 °C.

Polymer	Alkyne	Product	RCY (%)
Linear(N₃) polymer (9,253 g mol⁻¹)	3-Butyn-1-ol		71
Star(N₃) polymer (56,670 g mol⁻¹)	3-Butyn-1-ol		47
Linear(N₃) polymer (9,253 g mol⁻¹)	Butyne-Gd-DOTA		79
Star(N₃) polymer (56,670 g mol⁻¹)	Butyne-Gd-DOTA		58

Figure 4. Size-exclusion chromatograms for purified iodine-125/Gd-DOTA star polymer showing both absorbance at 256 nm and radio counts.

both 256 and 310 nm. Most importantly, the radioactivity detector showed a large signal at the same retention time as the nanoparticle, indicating successful iodine-125 radiolabelling for both the linear and star polymer nanoparticle. Subsequently, the radiochemical yield could be quantified by integrating both peaks and referencing back to injected amounts. The linear polymer had a higher RCY of 70.9% compared to 46.7% for the star polymer nanoparticle (see Table 2). The radiodetector also showed the presence of a small side product with a retention time of 34 minutes (RCY 2.9% for star polymer reaction). Based on the hypothesized reaction pathways of the three-component reaction[30] and the long retention time, this peak was attributed to [^{125}I]iodo-butynol, and this side-product could be easily removed by centrifugal filtration.

Having established a successful protocol for assessing the radiochemical yield of radioiodine labelled star polymer nanoparticles, we continued with the more complex three-component reaction with butyne-Gd-DOTA. Again, we tested the azide-functional linear polymer as well as the star polymer nanoparticle, and both were detected with a high radiochemical yield (See Table 2). Finally we were able to purify the 125-iodine/Gd-DOTA star polymer nanoparticle by centrifugal filtration (see Figure 4 and S18).

Conclusions

In this study, we successfully developed a bimodal core-cross-linked star polymer nanoparticle that contains both an MRI contrast agent (Gd-DOTA) and a radioisotope for nuclear medicine (^{125}I) using a one-pot three-component reaction. The use of radioisotopes of iodine allows a range of applications to be accessed: [123]I for SPECT imaging, [124]I for PET imaging, and ^{131}I for radioimmunotherapy. First, a chloride-functional star polymer nanoparticle was synthesized using the arm-first method. This was followed by the substitution of chloride with azide post-polymerization, creating an azide-functional core-cross-linked star polymer nanoparticle. Next the one-pot three-component (azide + alkyne + iodine) reaction was successfully optimized for macromolecules using a model system comprising an azide-functional linear or star polymer nanoparticle, a simple alkyne (3-butyn-1-ol) and cold sodium

iodide. It was shown that the iodine content could be tuned without affecting the conjugation efficiency. Subsequently the system was optimized for incorporation of the more complex butyne-Gd-DOTA, and MRI measurements showed an increased longitudinal relaxivity at 7 T compared to a commercial available small-molecule chelate. Finally, both linear and star polymers were successfully labelled with ^{125}I using 3-butyn-1-ol or butyne-Gd-DOTA. This bimodal radioisotope/MRI nanoparticle has a great potential to exploit the synergy between PET and MRI, and moreover combine MRI with radioimmunotherapy, thus creating a theranostic nanoparticle.

Conflicts of interest

There are no conflicts to declare.

Acknowledgements

References

1   R. Weissleder and M. J. Pittet, *Nature*, 2008, **452**, 580-589.
2   G. Mariani, L. Bruselli, T. Kuwert, E. E. Kim, A. Flotats, O. Israel, M. Dondi and N. Watanabe, *European Journal of Nuclear Medicine and Molecular Imaging*, 2010, **37**, 1959-1985.
3   M. D. Farwell, D. A. Pryma and D. A. Mankoff, *Cancer*, 2014, **120**, 3433-3445.
4   S. R. Cherry, A. Y. Louie and R. E. Jacobs, *Proceedings of the IEEE*, 2008, **96**, 416-438.
5   S. Vandenberghe and P. K. Marsden, *Physics in Medicine and Biology*, 2015, **60**, R115.
6   D. W. Townsend, *Physics in Medicine and Biology*, 2008, **53**, R1.
7   S. M. Ametamey, M. Honer and P. A. Schubiger, *Chemical Reviews*, 2008, **108**, 1501-1516.
8   E. Terreno, D. D. Castelli, A. Viale and S. Aime, *Chemical Reviews*, 2010, **110**, 3019-3042.
9   Z. Hu, W. Yang, H. Liu, K. Wang, C. Bao, T. Song, J. Wang and J. Tian, *Molecular Pharmaceutics*, 2014, **11**, 3798-3809.
10 W. P. Fendler, J. Czernin, K. Herrmann and T. Beyer, *Journal of Nuclear Medicine*, 2016, **57**, 2016-2021.
11 I. Santos, *Angewandte Chemie International Edition*, 2016, **55**, 35-35.

12 C. Kaittanis, T. M. Shaffer, A. Bolaender, Z. Appelbaum, J. Appelbaum, G. Chiosis and J. Grimm, *Nano Letters*, 2015, **15**, 8032-8043.

13 D. L. J. Thorek, D. Ulmert, N.-F. M. Diop, M. E. Lupu, M. G. Doran, R. Huang, D. S. Abou, S. M. Larson and J. Grimm, *Nature Communications*, 2014, **5**, 3097-3097.

14 R. M. Wong, D. A. Gilbert, K. Liu and A. Y. Louie, *ACS Nano*, 2012, **6**, 3461-3467.

15 R. Torres Martin de Rosales, R. Tavare, R. L. Paul, M. Jauregui-Osoro, A. Protti, A. Glaria, G. Varma, I. Szanda and P. J. Blower, *Angewandte Chemie International Edition*, 2011, **50**, 5509-5513.

16 H.-Y. Lee, Z. Li, K. Chen, A. R. Hsu, C. Xu, J. Xie, S. Sun and X. Chen, *Journal of Nuclear Medicine*, 2008, **49**, 1371-1379.

17 H. Yuan, M. Q. Wilks, M. D. Normandin, G. El Fakhri, C. Kaittanis and L Josephson, *Nature Protocols*, 2018, **13**, 392-412

18 E. Boros, A. M. Bowen, L. Josephson, N. Vasdev and J. P. Holland, *Chemical Science*, 2015, **6**, 225-236.

19 A. C. Anselmo and S. Mitragotri, *Bioengineering & Translational Medicine*, 2016, **1**, 10-29.

20 L. Frullano, C. Catana, T. Benner, A. D. Sherry and P. Caravan, *Angewandte Chemie International Edition*, 2010, **49**, 2382-2384.

21 J. Notni, P. Hermann, I. Dregely and H. J. Wester, *Chemistry*, 2013, **19**, 12602-12606.

22 C. Truillet, E. Thomas, F. Lux, L. T. Huynh, O. Tillement and M. J. Evans, *Molecular Pharmaceutics*, 2016, **13**, 2596-2601.

23 D. Kryza, J. Taleb, M. Janier, L. Marmuse, I. Miladi, P. Bonazza, C. Louis, P. Perriat, S. Roux, O. Tillement and C. Billotey, *Bioconjugate Chemistry*, 2011, **22**, 1145-1152.

24 J.-A. Park, J. Y. Kim, Y. J. Lee, W. Lee, S. M. Lim, T.-J. Kim, J. Yoo, Y. Chang and K. M. Kim, *ACS Medicinal Chemistry Letters*, 2013, **4**, 216-219.

25 M. de Smet, S. Langereis, S. van den Bosch, K. Bitter, N. M. Hijnen, E. Heijman and H. Grüll, *Journal of Controlled Release*, 2013, **169**, 82-90.

26 J. M. Ren, T. G. McKenzie, Q. Fu, E. H. Wong, J. Xu, Z. An, S. Shanmugam, T. P. Davis, C. Boyer and G. G. Qiao, *Chemical Reviews*, 2016, **116**, 6743-6836.

27 Y. Li, S. Laurent, L. Esser, L. V. Elst, R. N. Muller, A. B. Lowe, C. Boyer and T. P. Davis, *Polymer Chemistry*, 2014, **5**, 2592-2601.

28 J. Hu, R. Qiao, M. R. Whittaker, J. F. Quinn and T. P. Davis, *Australian Journal of Chemistry*, 2017, **70**, 1161-1170.

29 R. Yan, E. El-Emir, V. Rajkumar, M. Robson, A. P. Jathoul, R. B. Pedley and E. Årstad, *Angewandte Chemie International Edition*, 2011, **50**, 6793-6795.

30 R. Yan, K. Sander, E. Galante, V. Rajkumar, A. Badar, M. Robson, E. El-Emir, M. F. Lythgoe, R. B. Pedley and E. Årstad, *Journal of the American Chemical Society*, 2013, **135**, 703-709.

31 G. J. Strijkers, W. J. Mulder, G. A. van Tilborg and K. Nicolay, *Anti-cancer agents in medicinal chemistry*, 2007, **7**, 291-305.

32 32. M. Trollsås and J. L. Hedrick, *Journal of the American Chemical Society*, 1998, **120**, 4644-4651.

33 P. Caravan, *Chemical Society Reviews*, 2006, **35**, 512-523.

34 J. Ferreira, J. Syrett, M. Whittaker, D. Haddleton, T. P. Davis and C. Boyer, *Polymer Chemistry*, 2011, **2**, 1671.

35 S. Y. Khor, J. Hu, V. M. McLeod, J. F. Quinn, C. J. H. Porter, M. R. Whittaker, L. M. Kaminskas and T. P. Davis, *Journal of Pharmaceutical Sciences*, 2016, **105**, 293-300.

36 D. Lê, L. Liénafa, T. N. T. Phan, D. Deleruyelle, R. Bouchet, S. Maria, D. Bertin and D. Gigmes, *Macromolecules*, 2014, **47**, 2420-2429.

37 L. Esser, N. P. Truong, B. Karagoz, B. A. Moffat, C. Boyer, J. F. Quinn, M. R. Whittaker and T. P. Davis, *Polymer Chemistry*, 2016, **7**, 7325-7337.

38 R. J. Holbrook, N. Rammohan, M. W. Rotz, K. W. MacRenaris, A. T. Preslar and T. J. Meade, *Nano Letters*, 2016, **16**, 3202-3209.

39 I. M. Noebauer-Huhmann, P. Szomolanyi, V. Juras, O. Kraff, M. E. Ladd and S. Trattnig, *Investigative Radiology*, 2010, **45**, 554-558.

40 R. R. Carlton and A. McKenna-Adler, *Principles of Radiographic Imaging: An Art and A Science*, 5 edn., Cengage Learning, 2012.

Abstract Graphic